THE ASTROPHYSICAL JOURNAL, 253:353–366, 1982 February 1

OBSERVATIONS OF SOLAR FLARE TRANSITION ZONE PLASMAS FROM THE *SOLAR MAXIMUM MISSION*

CHUNG-CHIEH CHENG,[1] E. C. BRUNER,[2] E. TANDBERG-HANSSEN,[3] B. E. WOODGATE,[4] R. A. SHINE,[4] P. J. KENNY,[4] W. HENZE,[5] AND G. POLETTO[6]

Received 1981 March 23; accepted 1981 August 11

ABSTRACT

We present observations of the 1980 April 8 flare in the Si IV 1402 Å and O IV 1401 Å lines, obtained with the Ultraviolet Spectrometer and Polarimeter on *Solar Maximum Mission*. We have studied the spatial and temporal evolution of the Si IV, O IV intensity, density, and mass motions in the preflare and flare transition zone plasmas. The density is determined from the observed intensity ratio between the Si IV resonance line and the O IV intersystem line, and this diagnostic method is discussed in detail. The principal results are as follows: (1) The UV flare observed in the Si IV and O IV lines is unambiguously identified as occurring in a low-lying preexisting transition zone loop. The loop spanned the magnetic neutral line which separated a larger leader spot and a newly emerged isolated spot of opposite polarity. The loop became observable some 20 minutes before it flared, and it underwent slow brightness changes along its entire length with the most prominent changes at the top portion of the loop and at its westernmost footpoint near the leader spot. (2) At the onset of the flare, the easternmost footpoint, which was anchored in an isolated spot region of high longitudinal magnetic field gradient, suddenly showed impulsive brightening with large intensity increases. The impulsive brightening at this footpoint or kernel was correlated with an impulsive hard X-ray burst observed at the same time. This flaring kernel previously had been inconspicuous. (3) The density of the transition zone plasma at a temperature of $\sim 10^5$ K at the flaring footpoint increased an order of magnitude from its preflare value of 2×10^{11} cm^{-3} to 3×10^{12} cm^{-3} during the impulsive brightening. (4) The large intensity and density increases in the flaring kernel were associated with a downward mass motion with a velocity of ~ 20 km s^{-1}. The other part of the loop remained relatively stationary. (5) The emission from the high temperature flare plasma, as observed in the soft X-ray Fe XXV lines, was concentrated in a cloud overlying the whole Si IV/O IV loop, indicating that the flare energy was released in a low-lying loop or loops, including the observed Si IV/O IV loop. The released flare energy was transported by way of large-scale connecting field lines to other parts of the active region, producing the hot plasma and Hα kernels observed near the trailing spot. We discuss the implication of the preflare loop observations on flare mechanisms.

Subject headings: plasmas — Sun: flares — ultraviolet: spectra

I. INTRODUCTION

During the sudden energy release phase of solar flares, electromagnetic radiations are emitted in a wide wavelength range from radio to hard X-rays. It is known that soft X-ray bursts, which originate from a hot plasma at temperature $> 10^7$ K, consist of a rapidly rising phase with a time period of 5–10 minutes and a relatively longer gradual decay phase. In addition to the soft X-ray burst, there is enhanced emission from the cooler flare plasma with chromospheric and transition zone temperatures (10^4–10^5 K). Often, superposed on the soft X-ray rise phase, there is an impulsive or flash phase of very short duration, lasting 10–100 sec, during which impulsive hard X-ray, UV, and microwave bursts are produced. Recent studies of soft X-ray flare observations from *Skylab* and the P78-1 satellite have greatly increased our knowledge of the physical properties, the dynamical states, and the temporal evolutions of hot flare plasmas (Feldman, Doschek, and Kreplin 1980; Doschek *et al.* 1980; Moore *et al.* 1980). On the other hand, we know comparatively little about the physical conditions in the cooler chromospheric and transition zone plasmas, particularly in the preflare and the impulsive phases. This is partly due to the lack of UV observations with sufficient spatial resolution and complete time coverage. Previously Cheng (1978, 1980*a*), from *Skylab* observations, has shown that the enhanced UV emission is associated with enhanced density and large mass motions. Unfortunately, the *Skylab* UV observations were taken near or after the soft X-ray maximum in the gradual or decay phase. Thus, the physical conditions in the preflare transition zone plasmas and their spatial and temporal changes

[1] NASA Marshall Space Flight Center (now at E. O. Hulburt Center for Space Research, Naval Research Laboratory.
[2] Lockheed Palo Alto Research Laboratory.
[3] NASA Marshall Space Flight Center.
[4] NASA Goddard Space Flight Center.
[5] Teledyne Brown Engineering.
[6] Osservatorio di Arcetri, Italy.

during the rise and impulsive phases could not be adequately studied.

With the newly launched *Solar Maximum Mission* (*SMM*) satellite, it has now become possible to monitor a flare-productive active region continuously in UV and in soft and hard X-rays. In this paper, we present UV observations of the 1980 April 8 flare, with particular emphasis on the preflare and impulsive phases.

The observations were made in the UV emission lines of Si IV 1402 Å and O IV 1401 Å and were obtained with the Ultraviolet Spectrometer and Polarimeter (UVSP) on *SMM*. We derive, from the Si IV and O IV lines, the spatial and temporal evolution of density and mass motions in the transition zone plasmas ($\sim 10^5$ K) in the preflare stages as well as during the impulsive phase of the flare. The results show that, although there are intensity enhancements in various bright points in the 10^5 K plasma prior to the flare, the locations of the flare are unpredictable. That is, the UV flare kernels may or may not be the preflare bright points in the active region. The increase of UV intensity during the initial flare development is rather sudden and is impulsive in nature, correlating well in time with the impulsive hard X-ray bursts. The impulsive Si IV/O IV burst reaches its peak in a time scale of less than one minute. The intensity enhancement is accompanied by an equally drastic increase in density of more than one order of magnitude from its preflare active region value. Large mass motions are associated with the density increases.

In § II we discuss briefly the instrument, observational mode, and data analysis. The density diagnostic method using the Si IV/O IV line-intensity ratio is discussed in § III, and the observational results for the flare are presented in § IV. Finally, in § V we summarize and discuss the results.

II. INSTRUMENT AND DATA ANALYSIS

The UVSP instrument on *SMM* is a modified and improved version of the UV spectrometer flown on *OSO 8*. An added feature in the UVSP instrument is a polarimeter, capable of measuring polarization in various UV emission lines and the magnetic field in the chromospheric and transition zone. Basically, the UVSP instrument consists of a Gregorian telescope and an Ebert-Fastie spectrometer, which record solar spectra in the wavelength range 1170–3600 Å. It has many sets of slit combinations with various spatial and spectral resolutions and is capable of making spectroheliograms, dopplergrams, and spectral scans in one or more wavelength positions. A complete description of the UVSP instrument has been given by Woodgate *et al.* (1980). Some preliminary observational results on active regions and flares are presented by Tandberg-Hanssen *et al.* (1981) and Woodgate *et al.* (1981).

The flare observations studies in this paper were obtained in the raster-through-the-line (RL) mode, and with the slit set S. The size of the entrance slit in set S has a projected area on the Sun of 4″ × 4″ (2,900 × 2,900 km^2), and the width of the exit slits is 0.05 Å. The nominal wavelength positions of the exit slits in set S fall on the Si IV 1402.77 Å line in detector 1 and the O IV 1401.16 Å line in detector 4.

The RL mode consists of making spectroheliograms in a number of wavelength positions sucessively for a given line or lines of interest. The flare observations studies in this paper were taken with five wavelength positions: two on the red wing, two on the blue wing, and one at the center of the Si IV or O IV line. The distance between each wavelength position, $\Delta\lambda$, is 0.125 Å. The flare was observed with a 15 × 15 element raster, i.e., a 60″ × 60″ FOV, with a time cadence of 153 s for a complete RL mode.

For determination of density, the total intensities under the Si IV and O IV line profiles are required. This is done by summing the intensities recorded at the five wavelength positions for each of the 4″ × 4″ pixels. Since the raster at each wavelength position is done consecutively in time, the total intensity thus obtained is the averaged intensity under the line profile over the time interval of about 120 s for a 60″ × 60″ size raster. In addition to the density diagnostics from the simultaneous Si IV, O IV observations, the RL mode also yields information on the macroscopic velocity field distribution in the active region. This is because a crude line profile can be reconstructed from the RL data.

A complication on the use of the RL mode to deduce mass motion velocities occurs when the line intensity changes considerably during the completion time of the RL mode, such as during a flare. This is because the observations in the five wavelength positions, which are separated by the time required to make each raster, result in a distorted line profile due to the intensity variation. In this case, although it is more difficult to determine precisely the mass motion velocity than in a more quiescent situation, it is still possible to gain valuable information on the mass motions by comparison of the adjacent red and blue intensities from consecutive sets of the RL mode.

With the above discussion in mind, we derive the velocity from the RL mode as follows. For each raster element, a line profile can be constructed from the intensities recorded at the five wavelength positions. Let I_i denote the intensity at the wavelength position λ_i, where $i = 1, \ldots, 5$, increasing from the blue wing to the red wing. Since the reference wavelength position can be entirely arbitrary, we can for simplicity take $\lambda_1 = 0$ for the first wavelength position on the blue wing. Thus $\lambda_i = (i-1)\Delta\lambda$, where $\Delta\lambda = 0.125$ Å is the wavelength interval in the RL mode. Taking the first moment on the intensity, we calculate the line center position, λ_c, by

$$\lambda_c = \frac{\sum_{i=1}^{5} \lambda_i I_i}{\sum_{i=1}^{5} I_i} . \quad (1)$$

When this is done for each element in the 15 × 15 element raster, we obtain a spatially averaged line center, $\bar{\lambda}_c$. Finally, relative to $\bar{\lambda}_c$, the velocity at each element is given by:

$$v = c\frac{(\lambda_c - \bar{\lambda}_c)}{\lambda_0} , \quad (2)$$

where c is the speed of light and λ_0 is the center rest wavelength of the line. We stress that the velocity thus determined is relative to the whole region in the field of view. Although the absolute velocity cannot be determined accurately, the relative velocity measurement is useful for studying the velocity-shear distribution.

III. DENSITY DIAGNOSTIC USING THE Si IV/O IV LINE-INTENSITY RATIO

One of the important physical parameters of a plasma is the electron density. Basically, most of the methods involve the intensity ratio between an intersystem and an allowed line from a common ion. The use of line ratios from the same ion minimizes uncertainties in absolute intensity calibration, in atomic parameter calculations, and in the emission measure (EM) versus temperature distribution. Sometimes, however, suitable intersystem and allowed lines from the same ion cannot be found in the same wavelength region.

Recently, Feldman, Doschek, and Rosenberg (1977) have advanced the so-called O IV technique for density diagnostics of UV-emitting plasmas. They show that the intensity of any of the O IV intersystem lines, $2s^2 2p\ ^2P$–$2s2p^2\ ^4P$, combined with suitable allowed lines formed at approximately the same temperature, can be used to determine the density in a manner that is not so sensitive to the temperature structure of the plasma. The density sensitivity comes from the density dependence of the populations in the upper metastable level of the intersystem transitions. The idea is to derive the emission measure ([EM]) at the O IV temperature independently from some suitable allowed lines such that the density-sensitive part in the O IV intensity can be isolated. Specifically, they used the intersystem line O IV 1401 Å ($2s^2 2p^2 P_{3/2}$–$2s2p^2\ ^4P_{5/2}$), which is formed at 1.3×10^5 K, in combination with the allowed N V 1242 Å line ($\sim 1.8 \times 10^5$ K) and the C IV 1548 Å line ($\sim 10^5$ K). The [EM] of O IV is then obtained from the average of the C IV and N V [EM]'s. The averaging process somewhat takes into account automatically the [EM] distribution, thus partially alleviating the need for an atmospheric model. This diagnostic method has been applied to *Skylab* data for active region and flares (Feldman and Doschek 1978; Feldman, Doschek, and Rosenberg 1977; Cheng 1978, 1980*a*).

It is advantageous and straightforward to use the C IV and N V lines in the O IV technique if they can all be observed simultaneously, as in the *Skylab* UV spectra. Because of the difficulties of recording C IV, N V, and O IV lines at the same time by the UVSP instrument, U. Feldman (1978, private communication) suggested using the neighboring allowed Si IV 1402.7 Å line with the O IV 1401.2 Å line as a density diagnostic. Although Si IV is formed at slightly lower temperatures ($\sim 8 \times 10^4$ K) than the O IV line, the intensity ratio can nevertheless be used as a density diagnostic for the 10^5 K plasma, as we shall show below.

The emergent intensity of an allowed line, P_A, expressed in ergs s^{-1}, which is predominantly excited by electron collisions from the ground level, can be expressed in the effectively optically thin approximation as (cf. Feldman and Doschek 1978):

$$P_A = 2.2 \times 10^{-15} A_{\rm H}\, f_{\rm lu} \omega_l g_{\rm lu} [0.7 G(T_{\rm eA})] (N_e^2 \Delta V)_A\ , \tag{3}$$

where

$$G(T_{\rm eA}) = F(T_{\rm eA})(T_{\rm eA})^{-1/2} \exp\left(-\Delta E_{\rm lu}/kT_{\rm eA}\right)$$

and l, u are respectively the lower and upper levels of the transition, $A_{\rm H}$ is the element abundance relative to hydrogen, $f_{\rm lu}$ is the absorption oscillator strength, $g_{\rm lu}$ is the effective Gaunt factor, ω_l is the fraction of the ion population in level l, $T_{\rm eA}$ is the electron temperature of maximum emitting efficiency of the transition with energy $\Delta E_{\rm lu}$, $F(T_{\rm eA})$ is the fractional ion abundance in ionization equilibrium, N_e^2 is the averaged square density in the emitting volume ΔV, and k is the Boltzmann constant. Apart from the atomic and temperature factors, P_A is proportional to the emission measure, $N_e^2 \Delta V$, and can be expressed as

$$P_A = C_A G(T_{\rm eA})(N_e^2 \Delta V)_A\ , \tag{4}$$

where the constant C_A contains the atomic and other numerical factors. The function $G(T_{\rm eA})$, the so-called contribution function, is usually narrowly peaked with center at $T_{\rm eA}$ for most of the transition zone ions of interest. The emergent flux of an intersystem line or any other optically thin line, can be more conveniently and explicitly expressed as:

$$P_I = 0.8 A_{\rm H} A_{\rm lu} \Delta E_{\rm lu} [0.7 F(T_{\rm eI})] \left(\frac{N_u}{N_T}\right)_I (N_e \Delta V)_I\ , \tag{5}$$

where $A_{\rm lu}$ is the spontaneous decay rate for the transition, N_u is the number density of the upper level, and N_T is the total ion density, i.e., the sum of populations of all levels in the ion, and $T_{\rm eI}$ refers to the formation temperature of the intersystem line. Including all the atomic and numerical values in the constant C_I, equation (5) reduces to

$$P_I = C_I F(T_{\rm eI}) \left[\frac{J(N_e)}{N_e}\right]_I (N_e^2 \Delta V)_I\ , \tag{6}$$

where $J(N_e) = N_u/N_T$ is density dependent. The intensity ratio of the allowed to the intersystem lines is then from equations (4) and (6):

$$R = \frac{P_A}{P_I} = \frac{C_A G(T_{\rm eA})}{C_I F(T_{\rm eI})} \frac{(N_e^2 \Delta V)_A}{(N_e^2 \Delta V)_I} \left[\frac{J(N_e)}{N_e}\right]_I^{-1}\ . \tag{7}$$

Now, if the allowed and the intersystem lines are formed at the same temperature, $T_{\rm eA} = T_{\rm eI}$, then $(N_e^2 \Delta V)_A = (N_e^2 \Delta V)_I$, and their ratio depends only on the density sensitive term $[J(N_e)/N_e]_I$. From a comparison of the observed ratio with the calculated theoretically at various densities, the density in the emitting plasmas can be derived. If, on the other hand, the lines used are not formed at the same temperature, but at nearby temperatures, the situation becomes more complicated as in the case of the Si IV 1402 Å and O IV 1401 Å lines. However, if $[{\rm EM}]_{\rm A}$ at $T_{\rm eA}$ is related to the $[{\rm EM}]_I$ at $T_{\rm eI}$ by a constant,

$(N_e{}^2\Delta V)_A = \alpha(N_e{}^2\Delta V)_I$, where α is independent of density, then R becomes

$$R = \frac{C_A G(T_{eA})}{C_I F(T_{eI})} \propto \left[\frac{J(N_e)}{N_e}\right]_I^{-1} . \quad (8)$$

Again, R depends only on the density sensitive term $[J(N_e)/N_e]_I$, even though now the atomic factors for the two lines used are evaluated at slightly different temperatures. Notice that the density determined from equation (8) is for the temperature T_{eI}.

Feldman and Doschek (1978) have demonstrated from *Skylab* UV observations of active region and solar flares that the emission measures of the Si IV 1402 Å and the intersystem O IV 1401 Å lines are indeed proportional to each other. Thus, the Si IV/O IV ratio, as applied to equation (6), can be used for density diagnostics.

In order to use the Si IV/O IV ratio as a density diagnostic for solar transition zone plasmas more accurately, it is necessary to calibrate its variation with density. This we have done using the *Skylab* data (Feldman and Doschek 1978; Feldman, Doschek, and Rosenberg 1977). The solid curve in Figure 1 is the empirical density curve. It is obtained by plotting the observed Si IV 1402 Å/O IV 1401 Å line-intensity ratio from *Skylab* against the density values determined from the C IV, N V, and O IV lines for various active regions and flares. We see the Si IV/O IV ratio levels off at about 3 for densities lower than $\sim 3 \times 10^{10}$ cm^{-3}, the low density limit below which the ratio becomes insensitive to density. The ratio increases monotonically without limit at higher densities until laboratory densities are reached, thus making it especially useful for high density regions, such as in active regions and flares. To verify the empirical curve, we also calculated the Si IV/O IV ratio, using known atomic data and assuming $[EM]_{Si\ IV} = [EM]_{O\ IV}$. The dashed curve in Figure 1 shows the theoretical results. The Si IV 1402 Å line intensity is calculated at the Si IV ionization equilibrium temperature of $T_{eA} = 8 \times 10^4$ K, and the O IV 1401 Å line intensity is calculated at the O IV ionization equilibrium temperature of $T_{eI} = 1.2 \times 10^5$ K. We see immediately that the theoretical curve, which does not include solar abundances and other numerical factors, is parallel to the empirical curve. This indeed indicates that the observed Si IV emission measure is proportional to the O IV emission measure; the proportionality constant can be obtained by shifting the two curves horizontally until they coincide. Since the Si IV/O IV method is based empirically on the C IV, N V, and O IV method, it takes into account to a certain degree the atmospheric structures of the transition zone plasmas. It is difficult to assess the uncertainties of the Si IV/O IV method; we estimate that it gives a density measurement with an accuracy of about a factor of 2 or 3.

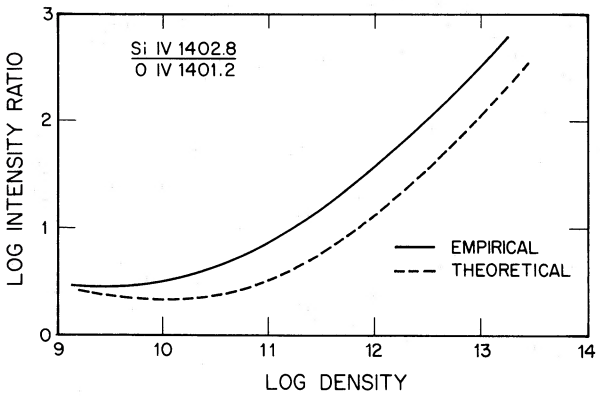

FIG. 1.—The solid curve, showing the empirical Si IV/O IV intensity ratio as a function of electron density, is derived from *Skylab* data, as explained in the text. The dashed curve is the theoretical intensity ratio calculated by using only atomic data without taking into account the relative solar abundance and emission measures of the Si IV and O IV ions. That the two curves are parallel indicates that the emission measures of the Si IV and O IV ions in solar flares are indeed proportional to each other. The empirical curve is used in the paper for density determination. Note that the density diagnostic method is good for plasmas with $N_e > 5 \times 10^{10}$ cm^{-3}.

We have checked the Si IV/O IV density diagnostic against densities derived from the intensity ratio O IV 1399 Å/O IV 1401 Å, which is also sensitive to density, but much less so than the Si IV/O IV ratio (Flower and Nussbaumer 1975). In the Si IV/O IV observational sequences obtained with the UVSP, we first made a spectral scan from 1390 Å to 1405 Å to locate the strong Si IV 1402 Å line within this spectral range. This is the so-called λ-max scan. The λ-max spectral scan takes about 6 minutes to complete and includes the O IV 1399 Å and 1401 Å lines. Although these lines are weak and their intensity ratio is density sensitive only in the range from 3×10^{10} to 2×10^{11} cm^{-3}, their ratio can nevertheless be used as a cross-check of the Si IV/O IV ratio. We have chosen more than 50 good λ-max scans which contain the O IV 1399 Å and 1401 Å lines with sufficient count rate for density comparisons. We find, except in those few obvious cases for which there were rapid brightenings during the 6 minute time span of the scan at the locations in active region where the λ-max scans were made, that the densities determined from the Si IV/O IV ratios agrees to within a factor of 2 or 3 with the densities determined from the O IV 1399 Å/1401 Å ratios.

In the following, we apply the methodology described above to the 1980 April 8 flare. In particular, we emphasize the preflare UV observation which is the first such observation in transition zone plasmas with high spatial resolution.

IV. OBSERVATIONS OF THE 8 APRIL 1980 FLARE

The active region 2373 (NOAA designation), during its passage across the central parts of the solar disk in the period 1980 April 6–10, was active and produced many flares. On 1980 April 7–8, the region developed a complex magnetic field structure of the sunspot type $\beta\gamma\delta$ with the large leader spot of positive magnetic polarity separated from the trailing spot by an intrusion of a newly emerged bipolar magnetic region, as can be seen from the MSFC magnetogram taken at 2054 UT on 1980 April 7 (Fig. 2).

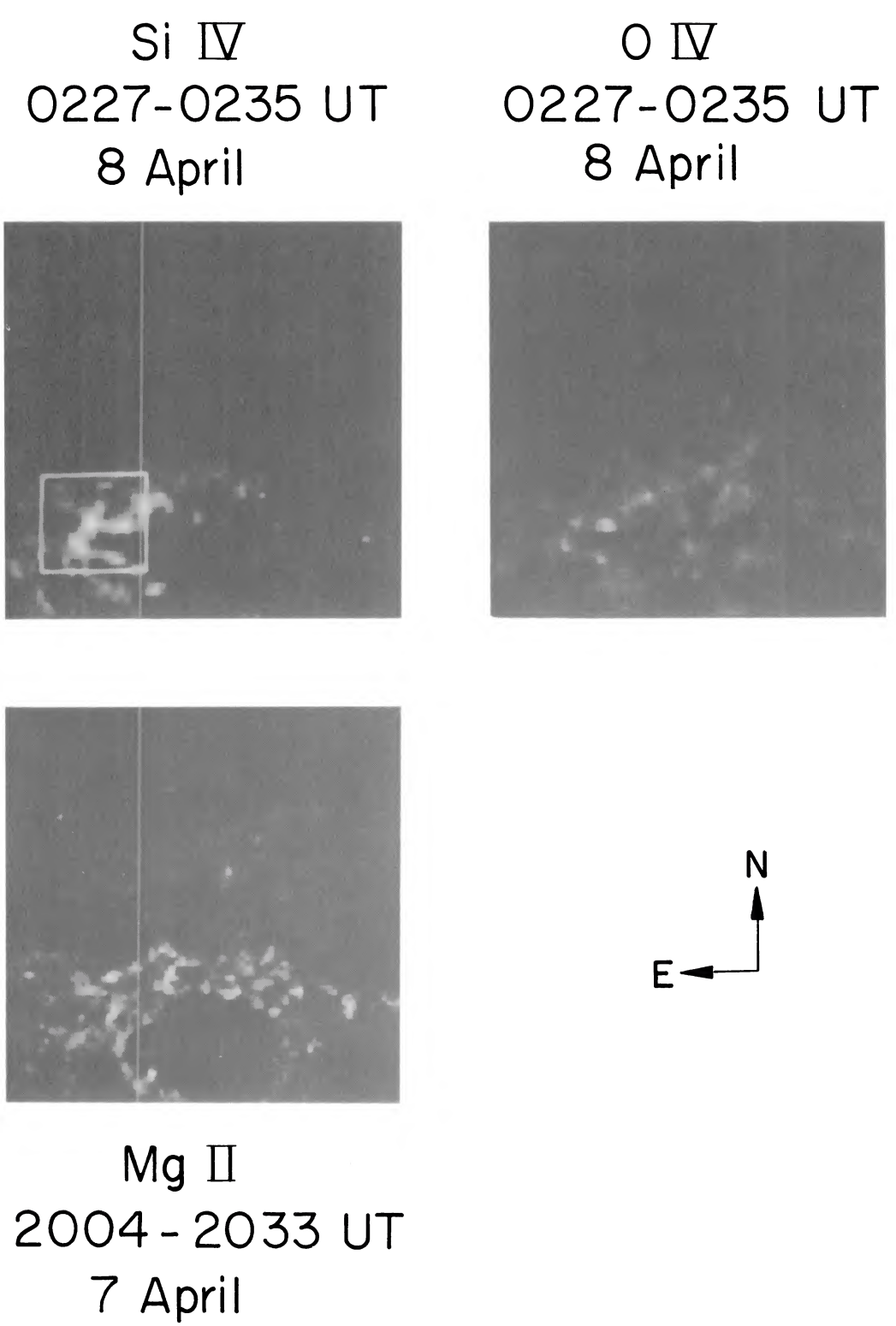

FIG. 2.—Si IV and O IV pictures of the active region AR 2372 with 4′ × 4′ FOV taken at the beginning of the satellite orbit. The pixel size is 4″ × 4″. The white inside square superimposed on the Si IV spectroheliogram shows the size (1′ × 1′) of the FOV and encloses the area of subsequent observations. The Mg II (~2800 Å) picture of the same active region with 4′ × 4′ FOV, taken some 4 hours before the Si IV/O IV pictures, shows the sunspots. The pixel size for the Mg II observation is 3″ × 3″.

This magnetic intrusion resulted in a δ-shaped neutral line and high magnetic gradient. It was in this region of magnetic complexity that most flaring activities were produced.

The 1980 April 8 flare in AR 2372 (N12 W10) was optically 1B started at 0303 UT, reached maximum at 0310 UT, and lasted almost 40 minutes until its end at 0350 UT. The flaring region was observed by the UVSP in the Si IV/O IV RL mode with a 1′ × 1′ field of view from 0235–0303 UT. Unfortunately the RL mode was interrupted at 0303 UT, the flare X-ray maximum, and the UVSP pointing was moved away from the flaring kernels. Although we did not follow the flare for its entire evolution, the available observations provide important information on the physical state of the preflare transition zone plasmas.

a) Morphological Evolution

In the sequence of UVSP observations, we first made a 4′ × 4′ FOV raster of the active region in the Si IV and O IV lines (Fig. 2). Once this was done, the RL mode was then started with a 1′ × 1′ FOV, centered on the brightest point as shown by the square superimposed on the Si IV spectroheliogram (Fig. 2). In Figure 2, we also show the Mg II picture of the active region taken at 2004 UT by UVSP, together with the MSFC magnetogram taken at 2054 UT, both on 1980 April 7. By using the sunspot positions in the Mg II picture as an intermediate step, we can determine the locations of the Si IV emission features relative to the photospheric magnetic field distributions in the active region. The error in the coregistration procedure is estimated to be within $\pm 5''$.

Figure 3 shows the results of coregistration; the square

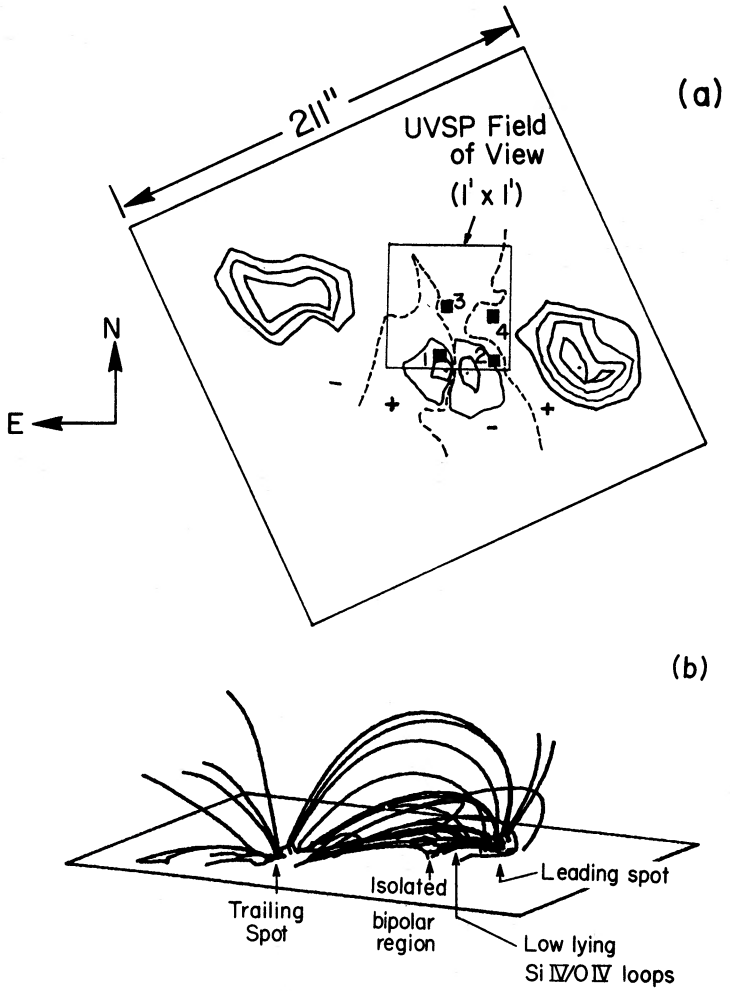

FIG. 3.—(*a*) Contour map, showing the distribution of the longitudinal magnetic field in the AR 2372, obtained with the MSFC vector magnetograph at 2054 UT on 1980 April 7. The dashed lines are the magnetic neutral lines. Notice that the small isolated emerging flux region, located between the large leader and trailing spots, is the location where many flares occured. The inside square locates the FOV (1′ × 1′) of the Si IV/O IV observations. The Si IV bright points observed at 0227 UT (see Fig. 2) are represented by small solid squares and are labeled 1, 2, 3, and 4. The pairs 1 and 2, 3 and 4 are identified as footpoints of two transition zone loops which bridge the magnetic neutral lines (see labels in Set 10, Fig. 4). (*b*) Potential field line calculations shown in three-dimensional perspective. Notice that the low-lying field lines, connecting the leader spot and the small isolated emerging flux region, can be identified with the Si IV/O IV loops, whose footpoints are indicated in Fig. 3*a*.

superposed on the longitudinal magnetic field distribution encloses the area of the active region covered by the 1′ × 1′ Si IV/O IV rasters, and the small black solid squares indicate the locations of the brightest points in the Si IV spectroheliogram as shown in Figure 2. Figure 3 shows that the pair of bright kernels, labeled 1 and 2, are situated on each side of the neutral line, which separates regions of opposite magnetic polarity. The same is true for the pair of bright points, labeled 3 and 4, just north of the kernels 1 and 2. Thus, the bright points 1 and 2, and 3 and 4, can be identified as the footpoints of two different transition zone loops. Indeed, a potential field line calculation (Fig. 3*b*, courtesy of Dr. S. T. Wu), based on the same MSFC magnetogram, shows low-lying loops connecting the big leader spot and the newly emerged isolated spot located just to the east. In addition, there are many large-scale loops connecting the leader spot and the trailing spot. The field-line structure has important implications on the soft X-ray and Hα emission distribution of the flare, as we shall see later. Therefore, we can unambiguously identify the Si IV/O IV bright kernels as the footpoints of the low-lying loops as indicated by arrows in the perspective pseudo–three-dimensional plot of the magnetic field structure (Fig. 3*b*). The connecting loops can be faintly seen in the Si IV spectroheliograms in Figure 2. We denote the loop whose footpoints are the kernels 1 and 2 as loop A, and the loop whose footpoints are the kernels 3 and 4 as loop B. As we shall see presently the flare occurred in the preexisting loop A, which became more conspicuous just before the sudden onset of the flare at 0303 UT.

Figure 4 shows the images of the active region in the Si IV and O IV lines with a 1′ × 1′ FOV observed from 0235 UT to 0303 UT. Included in Figure 4 are also density distributions, derived for each pixel from the Si IV/O IV line-intensity ratios. During the 28 minute period of observation before the flare onset, we obtained 11 complete sets of consecutive rasters, with each set consisting of five rasters at five wavelength positions, the time interval between each set being 153 s. The temporal variation of Si IV and O IV line intensities in loop A along its length is shown in Figure 5. The intensity map is arranged in the shape of the loop at 0302 UT (set 10) just before it flared. The intensity is the sum of count at the five wavelength positions and is therefore proportional to the total intensity under the Si IV or O IV line profile.

Examination of the morphological evolution of the Si IV/O IV emission features shows clearly that the flare occurred in a preexisting loop, loop A, particularly at footpoint 1 (Fig. 4). At 0235 UT, the bright point (kernel 3) in the center of the raster was the brightest feature in the FOV; the other kernels were relatively faint. Subsequently, the intensity of kernel 3 rapidly decreased by a factor of 10 and remained relatively unimpressive. At the same time, loop A began to brighten, starting at 0239 UT (set 2), particularly at the top portion. For the next 8 minutes there was little change in the morphology; the top portion of the loop remained the brightest feature. Then at 0247 UT the western footpoint (kernel 2 in the Fig. 3*a*) brightened by a factor of 2, while the intensity of the eastern footpoint (kernel 1) only increased very little. Five minutes later, at 0252 UT, the whole loop A began to brighten up, while the kernels just north showed no activity at all. At 0257 UT (set 9), loop A became more conspicuous. Just about 2 minutes (0259 UT) before the sudden onset of the flare, loop A was especially easy to recognize both in the Si IV and the O IV lines. The reason that loop A at this time was more easily seen is because the whole loop was at about the same brightness, while previously, there was a greater contrast between the different parts of the loop. The flare occurred suddenly at 0302 UT, with the Si IV brightness of footpoint 1 rapidly increasing by a factor of 8 or more. At the same time, there was relatively little change in the Si IV and O IV brightness at the other footpoints. It is, however, possible that other bright points outside the 1′ × 1′ FOV of our raster may have shown sudden brightness enhancements at the onset of the flare. At 0302 UT, when the Si IV intensity at kernel 1 was rapidly increasing, the other parts of the loop showed only a slight brightness enhancement. Notice that the intensity of the intersystem O IV line increased only about a factor of 2, in marked contrast to the allowed Si IV line. This is because of the large density at the flaring kernel.

Although the Si IV/O IV observation of the flare was interrupted at 0303 UT, when the flare intensity was still rising, we can deduce that the flare occurred in a preexisting loop (loop A). For 20 minutes before the sudden onset of the flare, the loop underwent gradual brightness variations in different parts. Since the transition zone plasma in the active region always evolves with time, it is not possible to ascertain whether the preflare brightness change observed in the loop is significant to the flare occurrence. That is, it is not possible to predict from the observed preflare activities in the transition zone plasma that a flare will follow.

b) Density and Mass Motions

The spatial distribution of the Si IV and O IV emissions is very similar, although the brightness contrast in the allowed Si IV 1402 Å line is much greater than that of the intersystem O IV 1401 Å line. This is largely due to density variation. The Si IV/O IV line-intensity ratio for the nonflaring active region is generally of the order of 10 (corrected for detector efficiency), giving a density of $2\text{–}5 \times 10^{11}$ cm^{-3}. In the normal course of active region evolution, a density variation of a factor of about 2 or 3 is a frequent occurrence. During the flare, the density of the flaring kernal increases drastically by more than a factor of 10. Figure 6 shows the temporal changes of density at various points along the length of the flaring loop A, as determined by the Si IV/O IV line-intensity ratio. It is clear that the large intensity enhancement in the Si IV emission at the time of flare onset at the footpoint is accompanied by an equally large enhancement in density. The density increases from its preflare value of 2×10^{11} cm^{-3} to about 3×10^{12} cm^{-3}. This is evidenced by an increase of more than a factor of 10 in the Si IV emission, while the O IV emission increases only by a factor of 2 at footpoint 1. On the other hand, the density at the other

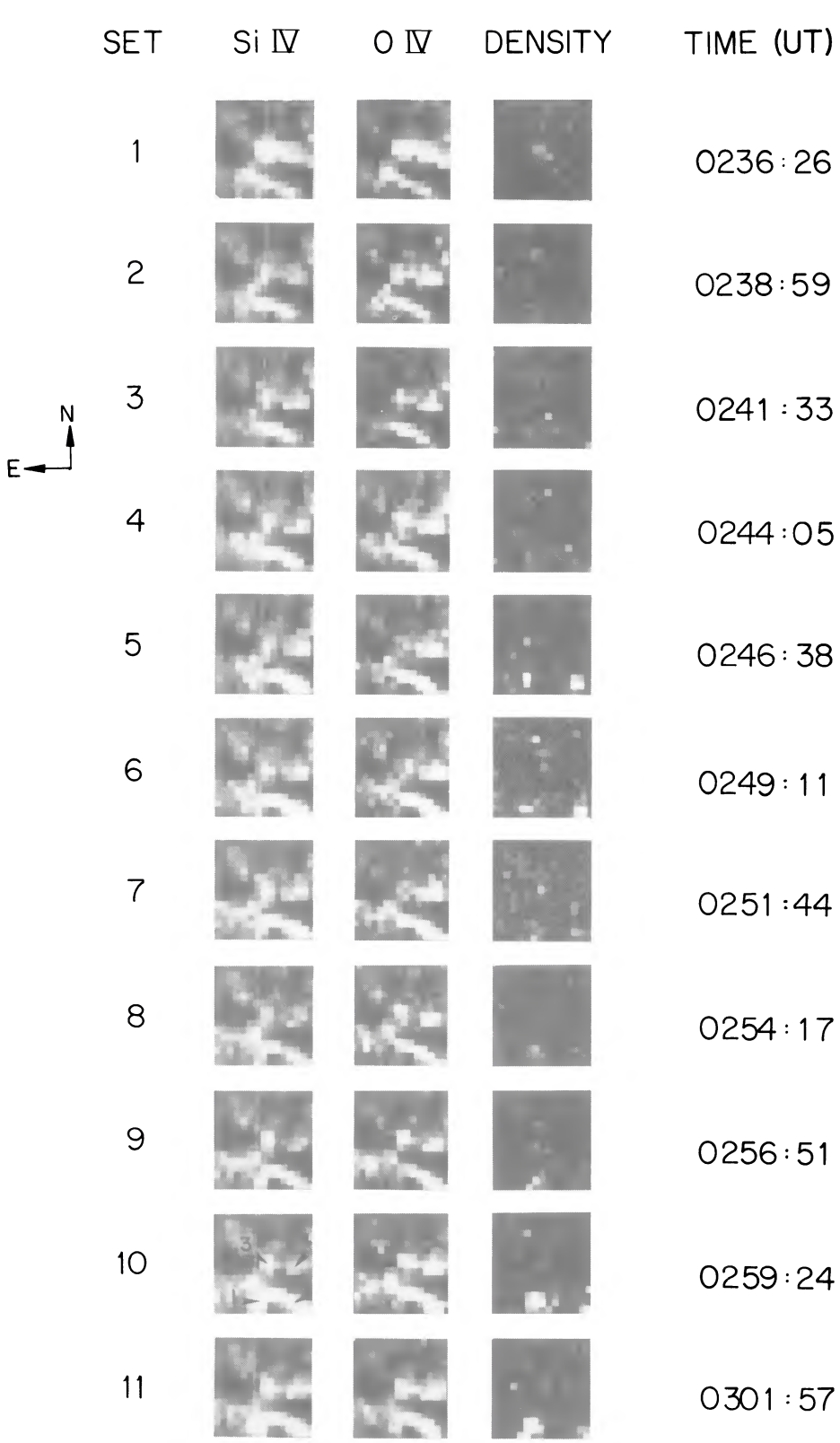

FIG. 4.—Evolution of the flaring region with a FOV of 1′ × 1′ as observed in the Si IV and O IV emissions in the period 0235–0302 UT. The pixel size is 4″ × 4″. The flare occurred in the last set (set 11) at 0302 UT. Notice the presence of the preflare Si IV/O IV loop and its morphological changes before the sudden onset of the flare with the impulsive brightenings at the footpoints (1 and 2). The loop connecting the kernels 1 and 2 is called loop A in the text. The spatial distribution of density is derived from the observed Si IV/O IV intensity ratios. Brighter areas have higher densities.

8 APRIL 1980 FLARE

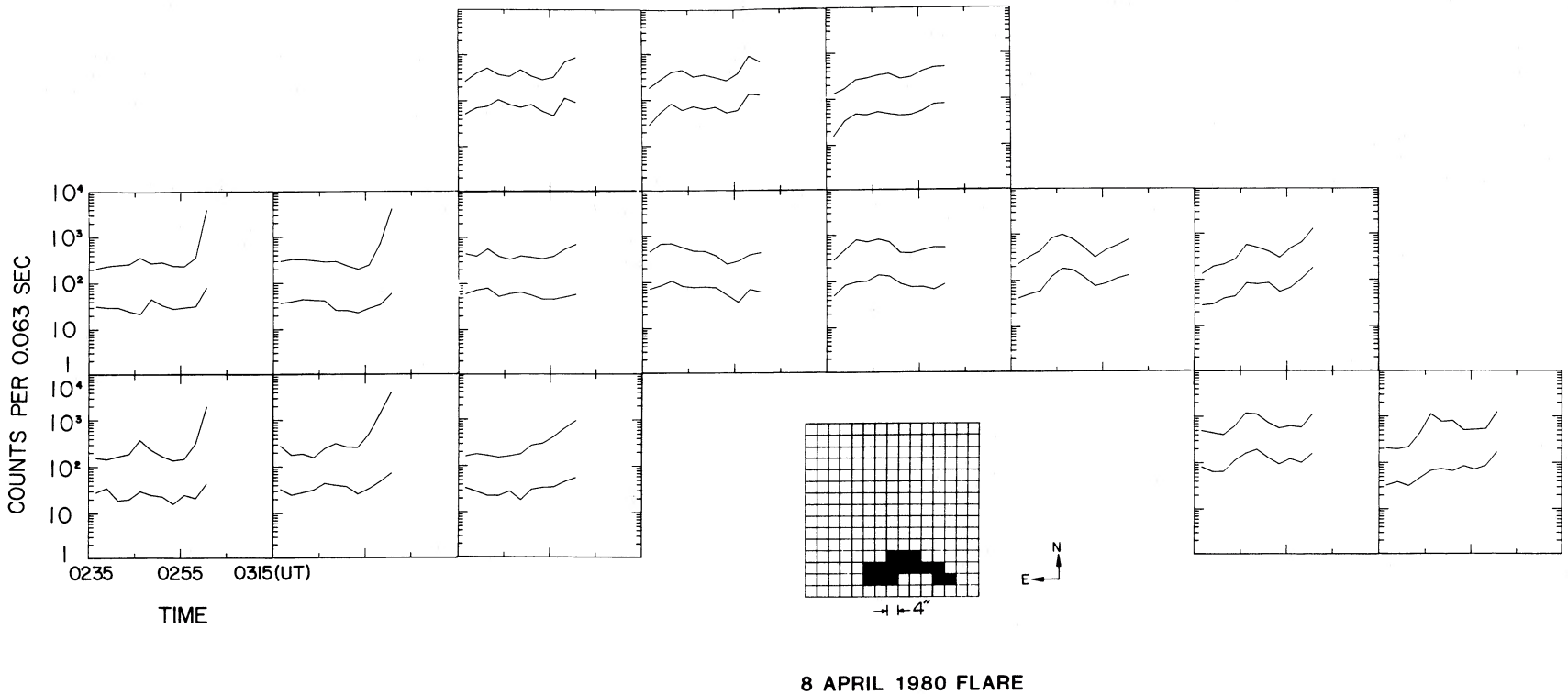

FIG. 5.—The intensity variations of the Si IV and O IV emissions in the flaring loop arranged in the shape of the loop (see Set 10, Fig. 4). The curves with largest count rates correspond to the Si IV line. The easternmost footpoint, showing the greatest intensity enhancement, is the brightest flaring kernel. Each square containing the curves represents a pixel.

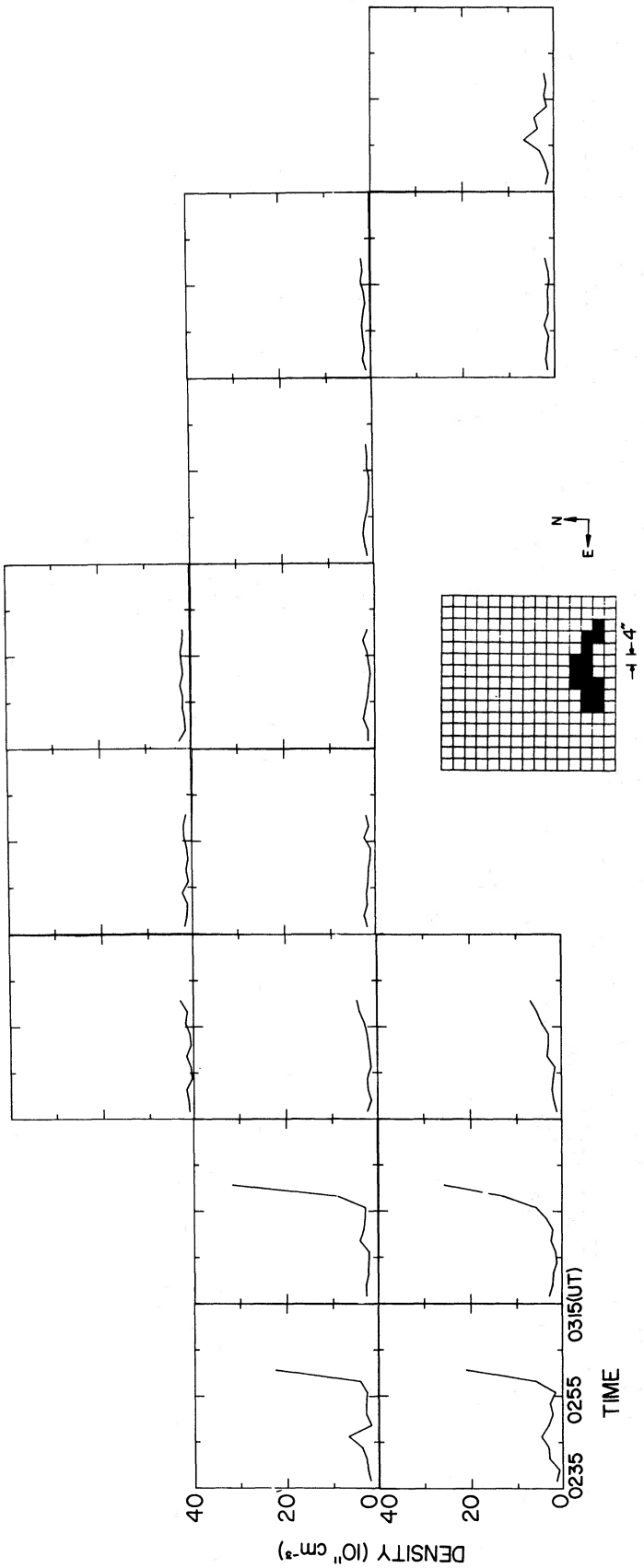

FIG. 6.—The temporal evolution of density along the flaring loop as derived from the Si IV/O IV intensity ratio, arranged, as in Fig. 5, in the shape of the loop. The density is greatly enhanced at the easternmost flaring kernels to a value of 3×10^{12} cm^{-3}.

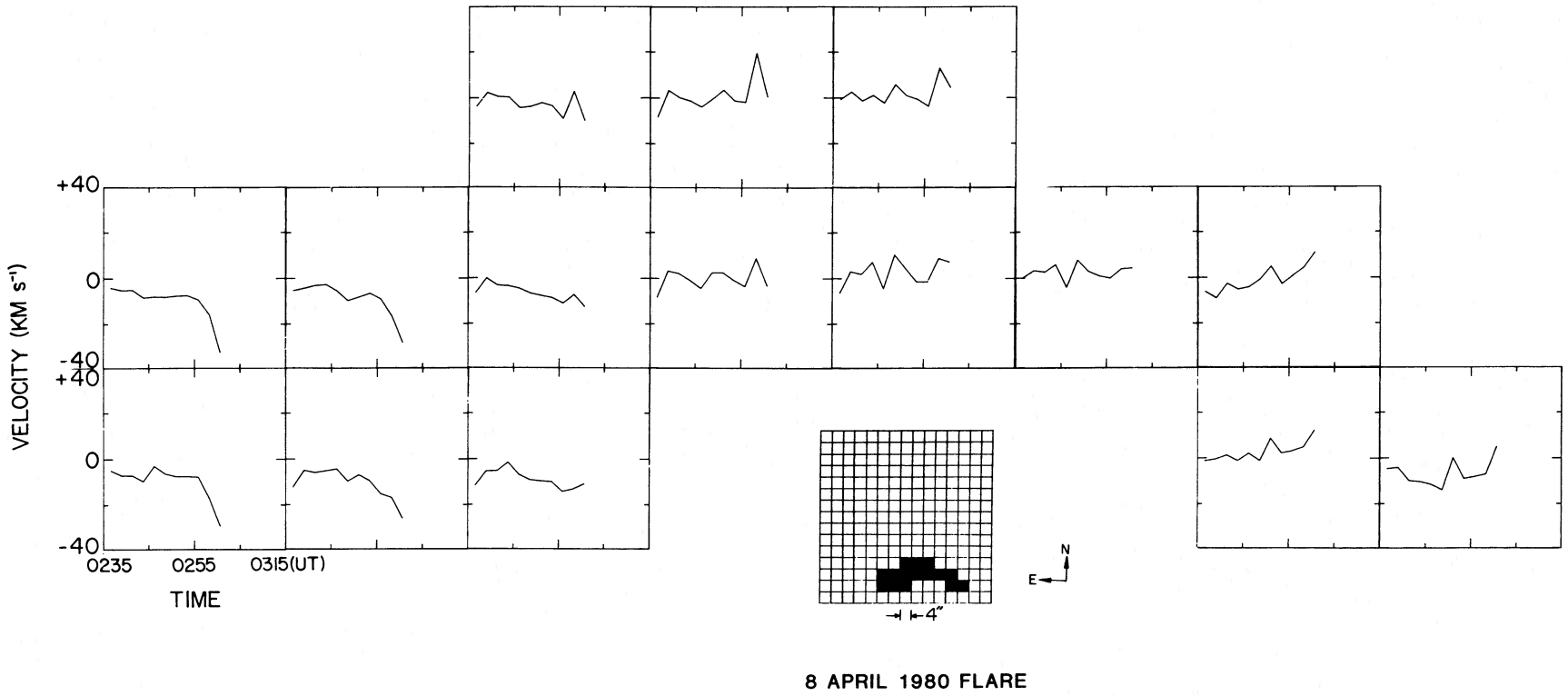

FIG. 7.—The temporal evolution of the mass motion along the flaring loop arranged in the shape of the loop. Most parts of the loop have no detectable mass motions, except at the eastern-most footpoint which shows a persistent downflow. At the onset of the flare the downflow velocity there increased to ~ 20 km s^{-1} (see text for details of velocity determination).

footpoint of loop A (kernel 2) as well as at the top of the loop shows very little temporal change. The density along most of the length of the loop remains at about 2×10^{11} cm^{-3}, its preflare value.

Using the velocity moment method as discussed previously, we have calculated, from the Si IV line, the mass-motion velocity as a function of time at different points along the length of the flaring loop A (Fig. 7). As before, the velocity map is arranged in the shape of a loop. Since the Si IV line is used, the velocity field derived is that of the lower transition zone plasma at $\sim 8 \times 10^4$ K. The reason that the Si IV line is used instead of the O IV line is that the greater Si IV intensity gives a better estimate of the velocity. Bruner (1981), from a Monte Carlo calculation of photon statistics, showed that the greater the observed total count, the smaller is the mass motion velocity that can be determined. Using Bruner's calculation for the C IV lines as a guide, we estimate that for the observed total Si IV line count of approximately 10^3, a velocity of about ~ 10 km s^{-1} should be measurable. Of course, this applies when the intensity does not change drastically. As Figure 5 shows, the Si IV and O IV intensities along the whole length of the loop A changed relatively little until 0257 UT, just before the sudden onset of the flare. Thus, the mass motion derived before this time should be representative of the actual mass motion velocity. We see from Figure 7 that there was a persistent downflow at the footpoint 1 before the onset of the flare, although there is a considerable uncertainty in its velocity, which was of the order of a few km s^{-1}.

At the beginning of the flare onset (0259 UT), the Si IV brightness at footpoint 1 and the downflow mass motion became much more pronounced; the velocity increased to ~ 20 km s^{-1}, accompanied by a density enhancement. Examination of the intensity of footpoint 1 observed in the next set of RL data (set 11) shows that the red-side intensities in set 10 (0259 UT) were much greater than the blue-side intensities in set 11, indicating that there was a large downflow mass motion. Another way of checking the validity of the mass motion is to combine the blue-side intensities in set 11 with the red-side intensities in set 10 in the velocity calculation. Indeed, we get consistent results with a downflow velocity of ~ 20 km s^{-1}. Additional support for the downflow comes from the calculation using the simultaneously observed O IV line, whose intensity enhancement at the flaring kernel is much less than that in the Si IV line. The result shows again a down flow mass motion with a comparable velocity to that from the Si IV observation.

c) *Relevant Observations in Hα, Soft, and Hard X-Rays*

So far, we have concentrated on the UVSP observations in the Si IV and O IV lines for the 1980 April 8 flare. The flare was observed also by other *SMM* instruments: in soft X-rays by the X-ray Polychromator (XRP), and in the hard X-ray energy range 25–140 keV by the Hard X-ray Burst Spectrometer (HXRBS). A complete analysis of the soft X-ray observations is in progress (Poletto *et al.* 1980); here, we briefly describe these observations relevant to our work.

The hard X-ray burst for the 1980 April 8 flare has two main peaks; the first was sharp and peaked at 0305 UT, and the second one was much broader and weaker and peaked at around 0306 UT (Orwig 1980). The highest energy channel which recorded the hard X-ray burst was in the range 96–140 keV. The burst started at 0303 UT, at which time the brightness of the Si IV emission at the flaring kernel was increasing rapidly, having reached a factor of 10 enhancement from its previous intensity. Although the Si IV/O IV observation was interrupted at 0303 UT, the Si IV flaring kernel can be associated with the first impulsive hard X-ray peak. In fact, Cheng *et al.* (1981) have recently shown from simultaneous observations that individual peaks in hard X-ray burst can be identified with impulsive brightenings at individual kernels in spatially resolved Si IV/O IV observations.

Soft X-ray spectroheliograms of the flare in the Fe XXV (1.85 Å), S XV (5.04 Å), and O VIII (18.97 Å) lines were made by XRP with a FOV of $4' \times 4'$, a spatial resolution of $15'' \times 15''$, and a time resolution of 4.3 minutes. We have coregistered the Si IV and the soft X-ray spectroheliograms by using the Mg II picture from UVSP and the on-board white light picture from XRP which both show the sunspot configurations. We estimate the accuracy to be $\pm 10''$ in the coregistration procedure between the Si IV and the soft X-ray spectroheliograms. At 0304 UT, the Fe XXV emission was at its peak intensity and was concentrated in a diffuse cloud with a dimension of $22''$. This high temperature plasma ($\sim 20 \times 10^6$ K) was located over the whole Si IV/O IV flaring loop, whose two footpoints were separated by about $24''$. While the Fe XXV emission was concentrated over the Si IV/O IV loop, which spanned the magnetic neutral line between the large leader spot and the isolated spot, the relatively cooler S XV ($\sim 16 \times 10^6$ K) and O VIII ($\sim 3 \times 10^6$ K) plasmas were distributed over a much wider area. In addition to a larger and more diffuse cloud containing the Fe XXV plasma, the S XV and O VIII lines also show an emission patch situated near the trailer spot, some $70''$ east of the Fe XXV plasma. Examination of the available Hα observation at 0322 UT in the postmaximum phase shows that there were four bright ribbons. The two Hα ribbons near the leader spot to the west can be associated with the Si IV flaring loop described before. The most eastern and extensive Hα ribbon near the trailer spot is cospatial with the eastern S XV/O VIII emission plasmas. It is clear that the source of the flare energy was located between the leader spot and the isolated spot, as evidenced by the Si IV flaring kernel and the high temperature Fe XXV plasma located there. The question, then, is how the S XV/O VIII plasmas and the Hα ribbons to the east were generated. The answer is contained in the magnetic field structure previously shown in Figure 3. As discussed above there are large scale, high field lines connecting the leader and the trailer spots, with smaller, low-lying loops underneath connecting the leader spot and the isolated spot. We submit that after the flare energy was released in the low-lying loops, i.e., the loops

we observed in the Si IV/O IV lines, energy and mass fluxes were then transported along the large scale loops to near the trailing spot, producing the hot plasmas and Hα ribbon there. By the same processes of energy transport along connecting field lines, the other Hα ribbons can be produced.

V. DISCUSSION

We have discussed the Si IV/O IV density diagnostic for transition zone plasmas. The underlying assumption is that the emission measure [EM] distribution as a function of temperature does not change drastically from flare to flare. That this is the case has been demonstrated by Feldman and Doschek (1978) from *Skylab* observations. Additional support comes from studies done by Emslie and Noyes (1978). They show from *Skylab* S055 data that a quantity directly related to the [EM] as a function of temperature has a similar shape not only during the rise and decay phases of a particular flare but also for different flares. Hence, the Si IV/O IV density diagnostic, although involving lines from two different ions, is nevertheless based on sound assumptions. The method is particularly valuable because it is the only suitable density diagnostic tool available for the UV flare plasmas observed by the *SMM*.

One of the principal results of the 1980 April 8 flare is the unambiguous identification of a low-lying transition zone loop as the site of the Si IV/O IV flare. The preflare loop had a length of 28″ and a diameter of ~ 4″. The loop spanned the magnetic neutral line which separated a large leader spot and a newly emergent isolated spot of opposite magnetic polarity. Previously, Schmahl *et al.* (1979) have observed a preflare UV structure bridging the neutral line which appears to be coincident with a flaring loop structure. With the good time coverage of the *SMM* observations, we are able to follow the evolution of the preflare transition-zone loop in the 1980 April 8 flare.

The Si IV/O IV loop began to be observable some 20 minutes before it flared, and it underwent slow brightness variations along its length. At the onset of the flare, the footpoints, particularly the easternmost one, suddenly brightened up, correlating temporally with the impulsive hard X-ray burst observed at the same time. The remainder of the loop showed only a relatively small intensity enhancement. We do not know whether the slow temporal and spatial variations in the preflare loop are characteristic precusors or just part of the evolutionary changes always associated with the normal course of an active region. However, we do know the physical parameters, such as density and mass motion, along the loop before it flared. The density in the Si IV/O IV loop along its length remained fairly constant with a value of $\sim 2 \times 10^{11}$ cm^{-3}. It was only at the impulsive flare onset that the density at the flaring footpoint increased by an order of magnitude to $\sim 3 \times 10^{12}$ cm^{-3}. The mass motion velocity along the loop was negligibly small, except at the easternmost footpoint where there was a persistent downflow of ~ 10 km s^{-1}. Thus, the preflare loop can be considered as quasi-static with a constant gas pressure of about 6 dyn cm^{-2}. This is about 3 times the gas pressure in an individual coronal loop with temperature of $\sim 2 \times 10^6$ K (Cheng 1980*b*). The high gas pressure in the Si IV/O IV loop requires a stronger confining azimuthal magnetic field than that in a corresponding coronal loop. This means that the confining magnetic field may be more twisted or sheared, and thus more susceptible to various plasma instabilities. The observation that the Fe XXV emission in the 1980 April 8 flare was concentrated in a cloud overlying the preflare Si IV/O IV loop, and that the Si IV/O IV brightening at the loop footpoint was temporally correlated with the hard X-ray burst, strongly suggest an energy source located in low-lying loops, including the one Si IV/O IV loop we observed.

Although the time resolution of the present UV observations does not permit us to compare in detail the temporal structures of the Si IV/O IV and the associated hard X-ray bursts, it is known that they are closely correlated (for a review, see Kane *et al.* 1980). In fact, Cheng *et al.* (1981) have recently shown from *SMM* observations that the UV bursts occur in discrete kernels where impulsive brightenings correlated temporally with different individual spikes in hard X-ray bursts. These spatially resolved UV observations are consistent with the *partial precipitation* model in which the UV burst is produced by high energy electrons impinging on a denser atmosphere (Kane 1974). Consequently, we conclude that the high energy electrons responsible for the Si IV/O IV and the hard X-ray emissions in the 1980 April 8 flare were accelerated in the preexisting preflare transition zone loop we observed. Since we do not know the acceleration mechanism of the energetic electrons, we will in the following estimates represent it by a large scale DC electric field. In order to be able to overcome collisional drag in the plasma and thus generate runaway electrons, this applied electric field must be greater than the critical Dreicer field E_D, which is given by (Dreicer 1959):

$$E_D = \frac{4\pi N e^3 \ln \Lambda}{kT_e},$$

where e is the electron change, k is the Boltzmann constant, and $\ln \Lambda$ is the Coulomb logarithm. With $N \sim 2 \times 10^{11}$ cm^{-3} and $T_e \sim 10^5$ K in the preflare loop, we obtain $E_D \sim 2.6 \times 10^{-4}$ statvolt cm$^{-1} \approx 8 \times 10^{-2}$ volt cm^{-1}. Therefore, an impressed electric field of at least the size of the Dreicer field is needed to accelerate ambient thermal electrons with temperature 10^5 K. Furthermore, this applied field must be operative over a length of $\sim 10^6$ cm in order to generate electrons with energy 100 keV. The length of the Si IV/O IV loop we observed was $28'' = 2 \times 10^9$ cm; thus, the acceleration region was only about 0.05% of the total length. If, however, the preflare loop was a coronal loop with temperature of $\sim 2 \times 10^6$ K and density of $\sim 4 \times 10^9$ cm^{-3} (Cheng 1980*b*), then the corresponding Dreicer field would be reduced by three orders of magnitude, while, at the same time, the dimension of the acceleration region would be increased by the same order of magnitude.

At the present time, most theoretical studies on the preflare state have assumed the physical conditions of a coronal loop (for a review, see Van Hoven *et al.* 1980). As we have seen in this paper, the preflare loop in the 1980 April 8 flare was, however, a transition zone loop with different physical parameters. It is, therefore, important for an understanding of flare mechanisms that studies of plasma instabilities in a preflare transition zone loop be undertaken. For example, the requirement of an acceleration mechanism may differ considerably for different physical conditions in a preflare loop. A transition zone loop requires a large electric field for acceleration of particles which may be difficult to obtain, but the source region is quite localized. On the other hand, for a coronal loop, a small applied field is satisfactory, but a large source region is required. This and other topics concerning the flare mechanism should be examined, with realistic physical conditions of a preflare loop like the ones presented in this paper.

It is impossible to list all the people who have contributed in various stages to the success of a large space endeavor such as the *Solar Maximum Mission*. Here we sincerely thank them all. For valuable discussions concerning this paper we are indebted to Dr. U. Feldman who suggested the density diagnostics used and to Dr. G. A. Doschek for further elucidations on this method. We would also like to thank Dr. M. Haygard for supplying the MSFC magnetogram and Dr. S. T. Wu whose magnetic field-line calculations contributed greatly to our understanding of the 1980 April 8 flare.

REFERENCES

Bruner, E. C. 1981, *Ap. J.*, **247**, 317.
Cheng, C.-C. 1978, *Solar Phys.*, **56**, 205.
———. 1980*a*, *Solar Phys.*, **65**, 283.
———. 1980*b*, *Ap. J.*, **238**, 743.
Cheng, C.-C., *et al.* 1981, *Ap. J.* (*Letters*), **248**, L39.
Doschek, G. A., Feldman, U., Kreplin, R. W., and Cohen, L. 1980, *Ap. J.*, **239**, 725.
Dreicer, H. 1959, *Phys. Rev.*, **115**, 238.
Emslie, A. G., and Noyes, R. W. 1978, *Solar Phys.*, **57**, 373.
Feldman, U., and Doschek, G. A. 1978, *Astr. Ap.*, **65**, 215.
Feldman, U., Doschek, G. A., and Kreplin, R. W. 1980, *Ap. J.*, **238**, 365.
Feldman, U., Doschek, G. A., and Rosenberg, F. D. 1977, *Ap. J.*, **215**, 652.
Flower, D. R., and Nussbaumer, M. 1975, *Astr. Ap.*, **45**, 145.
Kane, S. R. 1974, in *IAU Symposium 57, Coronal Disturbances*, ed. G. Newkirk, Jr. (Dordrecht: Reidel), p. 105.
Kane, S. R., *et al.* 1980, in *Solar Flares*, ed. P. A. Sturrock (Boulder: Colorado Associated University Press), Chap. 5, p. 187.
Moore, R., *et al.*, 1980, in *Solar Flares*, ed. P. A. Sturrock (Boulder: Colorado Associated University Press), Chap. 8, p. 341.
Orwig, L. E. 1980, private communication.
Poletto, G., *et al.* 1980, private communication.
Schmahl, E. J., Solodyna, C. V., Smith, J. B., Jr., and Cheng, C.-C. 1978, *Solar Phys.*, **60**, 323.
Tandberg-Hanssen, E., *et al.* 1981, *Ap. J.* (*Letters*), **244**, L127.
Van Hoven, G. A., *et al.* 1980, in *Solar Flares*, ed. P. A. Sturrock (Boulder: Colorado Associated University Press), Chap. 2, p. 17.
Woodgate, B. E., *et al.* 1980, *Solar Phys.*, **65**, 73.
Woodgate, B. E., *et al.* 1981, *Ap. J.* (*Letters*), **244**, L133.

E. C. BRUNER: Lockheed Palo Alto Research Laboratory, 3251 Hanover Street, Palo Alto, CA 94304

CHUNG-CHIEH CHENG: Code 4175CC, Naval Research Laboratory, Washington, DC 20375

W. HENZE: Teledyne Brown Engineering, Huntsville, AL 35807

P. J. KENNY, R. A. SHINE, and B. E. WOODGATE: Code 409, SMM/UVSP, Goddard Space Flight Center, Greenbelt, MD 20771

G. POLETTO: Osservatoria di Arcetri, Firenze, Italy

E. TANDBERG-HANSSEN: ES 51, Marshall Space Flight Center, AL 35812